UNCONVENTIONAL RESOURCES TECHNOLOGY CONFERENCE
FUELED BY SPE • AAPG • SEG

URTeC: 3854538

Analysis of Uniformity of Proppant Distribution Between Clusters Based on a Proppant-Wellbore Dynamics Model

Egor Dontsov*[1], Christopher Hewson[1], Mark McClure[1], 1. ResFrac Corporation.

Abstract

Limited entry technique is often employed to achieve uniform flow distribution between perforation clusters during hydraulic fracturing treatment. However, the proppant distribution between clusters will not necessarily be uniform, even if the slurry distribution is uniform. As the average slurry velocity reduces from one cluster to another, this leads to proppant settling and higher particle concentration in the lower portion of the wellbore. Also, the slurry makes a sharp turn to enter a perforation and the higher proppant density causes some particles to miss the perforation. These two physical effects are primarily responsible for the non-uniform proppant distribution between the clusters. In view of these observations, the purpose of this study is to investigate the degree of uniformity of proppant placement based on a recently developed proppant-wellbore dynamics model. A field scale case consisting of 13 perforation clusters is considered. Three perforation designs are compared: the original design with 3 perforations phased 120°, a case in which the orientation of each individual perforation shot is optimized, and a case in which phasing is optimized with the constraint that all perforations have the same orientation. The goal of the optimization procedure is to achieve more uniform proppant distribution. Results are presented in the context of uncertainty of perforation diameter and phasing. Finally, the effect of stress shadow from the previous stage on the variability of proppant placement is investigated. It is found that the optimal perforation phasing leads to a significantly more uniform proppant distribution between perforations and that the effect of stress shadow does not significantly alter the results as soon as sufficiently strong perforation friction is used. Uncertainty of perforation phasing and diameter introduces a certain level of variation to the results, but this level is noticeably smaller compared to the improvement achieved by using the optimal perforation orientation.

Introduction

Hydraulic fracturing treatments involve pumping particle laden slurry down the wellbore, which then enters the rock formation through a series of perforation holes that are typically arranged in clusters. It is desirable for the fluid and particle distribution between the perforations to be uniform, because this maximizes production and recovery factor. Fluid uniformity is typically achieved with the so-called limited entry technique, in which perforation pressure drop is designed to be sufficiently high to overcome variations of fluid pressure between different fractures (Cramer, 1987). Unfortunately, the

limited entry approach does not guarantee uniform particle distribution between the clusters. Because the propped surface area is essential for production, the amount of proppant received by each fracture directly influences profitability.

There are two mechanisms that contribute to non-uniform proppant distribution. The first mechanism is related to particle settling in the wellbore and is particularly important in horizontal wellbores. As soon as flow starts to encounter perforations, the average slurry velocity begins to slow down, which in turn reduces the ability of the flow to suspend proppant. This introduces a bias in proppant concentration, so that there is more proppant at the bottom of the wellbore. As a result, perforations located at the bottom of the well receive more proppant than their counterparts located at the top. The second mechanism is related to particle slip due to the contrast of particle and fluid densities. Slurry needs to make a sharp turn in order to enter the perforation, and, in particular, it needs to slow down in the horizontal direction. Because of their greater density, some particles are unable to complete the turn before entering the perforation and, consequently, some of them miss the perforation. This mechanism always reduces the amount of particles that enter the perforation, but the degree of the reduction depends on problem parameters.

Most of the studies that investigated this problem focused predominantly on the turning part of the problem, i.e., on the ability of proppant to turn from the wellbore to perforation. This includes experimental study Gruesbeck and Collins (1982), as well as Computational Fluid Dynamic (CFD) simulations by Wu and Sharma (2016); Wu (2018).

More recently, the problem of the whole perforated wellbore was investigated in laboratory setting (Ngameni et al., 2017; Ngameni, 2016; Ahmad and Miskimins, 2019a,b; Ahmad et al., 2021; Ahmad, 2020). On the other hand, field scale measurements are presented in Crespo et al. (2013); Kolle et al. (2022); Snider et al. (2022). What is found is that particle distribution between the perforation clusters can be non-uniform and that the result depends on many parameters, such as proppant size and fluid properties.

A model for proppant dynamics in the wellbore is developed in Dontsov (2023). The model is able to capture both the particle settling in the wellbore, as well as the physical mechanisms leading to proppant missing the perforation hole due to higher inertia. This model is calibrated against numerous laboratory data measurements and agrees well with both laboratory scale and field scale multi-cluster experiments. Further, the work Dontsov et al. (2023) presents the optimization algorithm that is based on this model. In particular, it is shown that it is possible to optimize phasing of each individual perforation to achieve much more uniform proppant distribution between perforations. Based on the model and the optimizer, the purpose of this study is to further extend the developments to address a practical problem of uncertainties. The goal is to quantify how the uncertainty of perforation diameter and azimuth affect the overall particle distribution for the original non-optimized and optimized scenarios.

Proppant-wellbore dynamics model

This section briefly outlines the proppant-wellbore dynamics model that is summarized in Dontsov (2023). Fig. 1*(a)* schematically shows a wellbore cross-section. Due to gravity, there is higher particle concentration in the lower part of the well. A perforation is located in the upper-right portion of the cross-section. Fluid streamlines located within the fluid ingestion zone enter the perforation. The size of this zone primarily depends on the ratio between the fluid flow rate in the wellbore and the fluid flow rate in the perforation. For the very first perforation in the stage (heel), the size of the fluid ingestion zone is small, while for the very last perforation (toe), the size of the fluid ingestion zone is equal to the whole wellbore since all the remaining fluid flows through the last perforation. The proppant ingestion zone is always smaller than its fluid counterpart because particles have higher mass density and tend to miss the perforation. The ratio between the proppant and fluid ingestion zones determines the turning efficiency.

The efficiency is equal to 1.0 when the two ingestion zones coincide. Typically, the efficiency ranges from 0.7 to 0.9 (Dontsov, 2023).

Fig. 1*(b)* illustrates an important practical issue related to the definition of perforation phasing. In the field, the latter is defined relative to the center of the perforation gun. But the gun itself has a diameter smaller than the wellbore and it lies at the bottom of the well. Therefore, the azimuth relative to the center of the well θ_{well} and the corresponding azimuth calculated relative to the center of the gun θ_{gun} are different. Given the ratio between the perforation gun and wellbore diameters, the different phasing definitions can be converted as

$$\theta_{well} = \theta_{gun} + sin^{-1}\left(rsin(\theta_{gun})\right), \theta_{gun} = tan^{-1}\left(\left(r + cos(\theta_{well})\right)^{-1} sin(\theta_{well})\right), r = 1 - \frac{d_{gun}}{d_{well}}. \quad (1)$$

In the above, conversions care must be taken to ensure that the angle falls into the correct quadrant.

Fig. 1*(c)* shows particle volume fraction distribution in the well predicted by the model. The single parameter that quantifies the ability of flow to suspend particles is called dimensionless gravity:

$$G = \frac{8\phi_m(\rho_p - \rho_f)g d_w}{f_D \rho_f v_w^2}. \quad (2)$$

Here $\phi_m = 0.585$ is the maximum volume fraction of particles, ρ_p is particle mass density, ρ_f is fluid mass density, $g = 9.8$ m/s^2 is gravitational constant, d_w is wellbore diameter, $f_D = 0.04$ is fitting parameter that can also be interpreted as a friction factor in the pipe, and v_w is the average wellbore velocity. All the parameters, except the wellbore velocity remain the same within the given stage. For the heel perforations when the velocity is high, the value of the parameter G is low (on the order of 1 for field scale parameters), and therefore the proppant distribution is nearly uniform. At the same time, velocity drops significantly for toe perforations and the dimensionless gravity G can reach 100, which results in significantly asymmetric particle distribution in the wellbore in which particle motion corresponds to the "flowing bed" state.

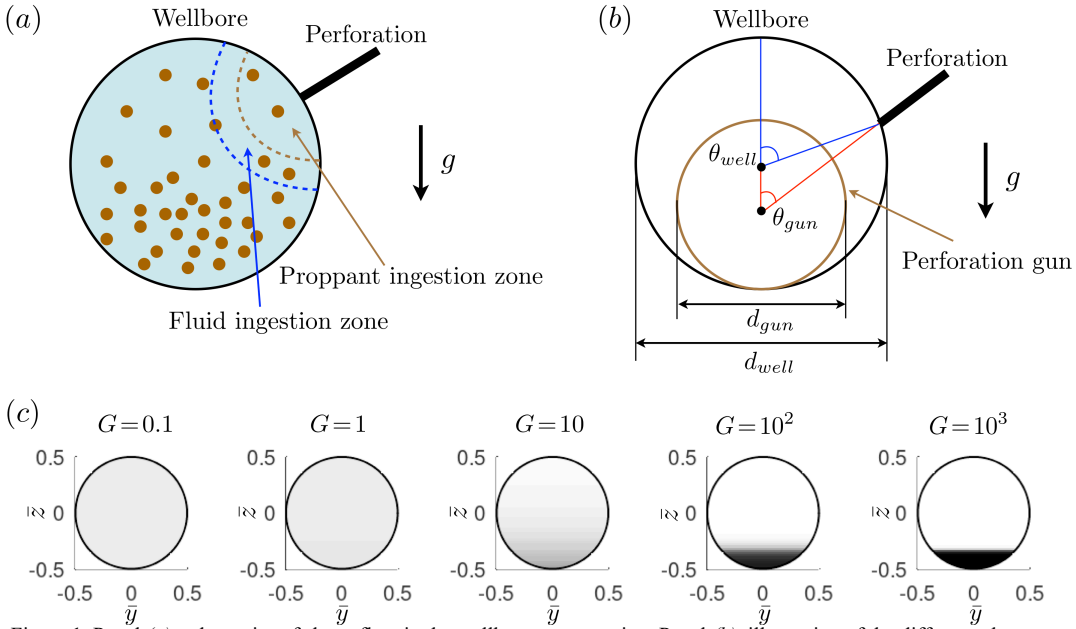

Figure 1. Panel *(a)*: schematics of slurry flow in the wellbore cross-section. Panel *(b)*: illustration of the difference between wellbore centered azimuth and perforation gun centered azimuth. Panel *(c)*: numerical simulations of particle concentration in the wellbore for different values of the dimensionless gravity G.

Illustrations presented in Fig. 1 already allow us to qualitatively understand how perforation orientation can influence particle distribution. In the heel part of the stage, where the values of the dimensionless gravity G are small, the particle distribution is nearly uniform and therefore the perforation orientation

does not affect the result. At the same time, in the middle of the stage, and especially close to the toe, there is significant effect of proppant settling and therefore perforation azimuth becomes important. Perforations that are located at the top of the well receive less proppant, while the ones located at the bottom receive more proppant. As discussed in Dontsov (2023), the use of 60° or 90° phasing allows to promote uniformity by effectively averaging over various orientations, but it does not completely solve the problem of uniform proppant distribution.

The developed wellbore proppant dynamics model is calibrated against two sets of data. The first set of data is related to the problem of slurry flow in a pipe and particle settling. Laboratory experiments for such a problem were performed in Gillies (1993). Fig. 2 shows the comparison between the measurements and the model. In total, there are 73 cases corresponding to different pipe diameters, particle concentrations, fluid velocities, and particle sizes. Only three cases are selected for detailed omparison, see Fig. 2*(a)* and *(b)*, while the error for all the cases is plotted in Fig. 2(c). Here $\overline{z}$ is the normalized vertical coordinate so that $\overline{z} = 0.5$ corresponds to the top of the pipe, while $\overline{z} = -0.5$ represents the bottom. The particle volume fraction is denoted by ϕ, while the velocity is v_w. As can be seen from the figure, both the particle volume fraction and the velocity are captured well by the model. In addition, the particle concentration is very non-uniform for some cases and the flow indeed approaches the "flowing bed" state for some parameters.

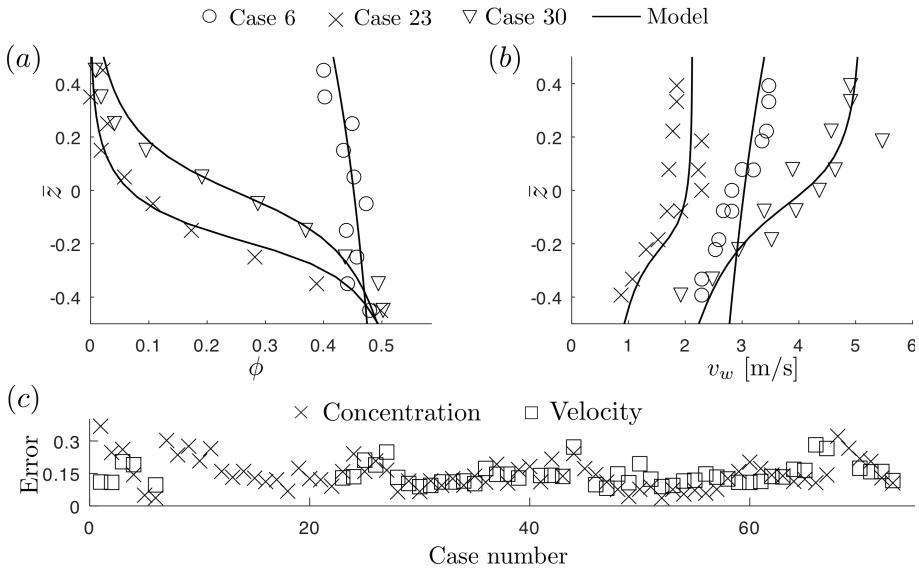

Figure 2. Comparison between the model and laboratory measurements (Gillies, 1993). Panel *(a)* shows the comparison of particle distribution in a pipe. Panel *(b)* shows the comparison of velocity distribution in a pipe. Panel *(c)* summarizes the error for all 73 cases.

Calibration and validation are also performed for the sub-problem of particle turning into a perforation. Such a problem is schematically shown in Fig. 3*(a)*. The inlet slurry and proppant flow rates q_i^s and q_i^p are given. The perforation slurry flow rate q_p^s is also given. The goal is to obtain the perforation particle rate q_p^p, as well as the flow rates at the outlet, q_o^s and q_o^p. Fig. 3*(b)* and *(c)* compare model predictions to CFD simulations in Wu and Sharma (2016) for various parameters. Here, d_w is wellbore diameter, θ is perforation azimuth relative to the wellbore center, $\langle\phi\rangle$ is the average particle concentration, μ is fluid viscosity, d_p is perforation diameter, a is the particle radius, while ρ_p is particle density. The figures plot the proppant flow rate ratio versus the slurry flow rate ratio. In addition, Fig. 3*(c)* plots the same quantities, but for the experimental data from Gruesbeck and Collins (1982). As can be seen from the results, the model is able to accurately match both laboratory measurements, as well as CFD simulations. The dashed line corresponds to the turning efficiency of one, i.e., when particles do not slip relative to the fluid. More comparisons can be found in Dontsov (2023).

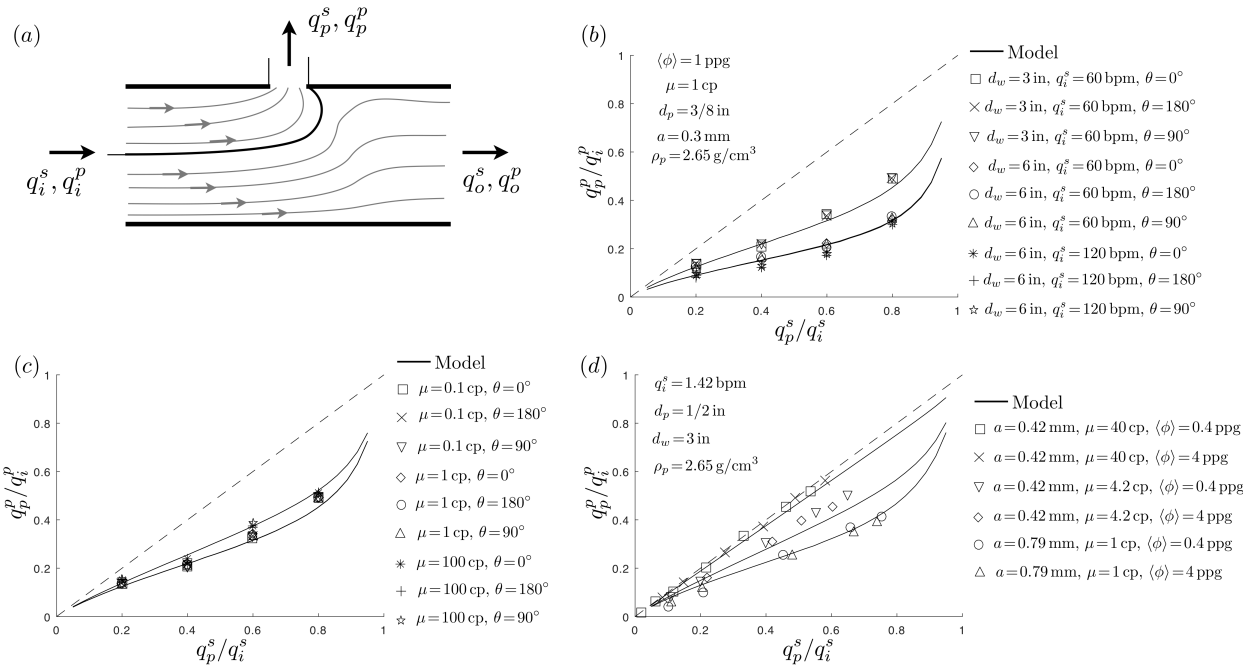

Figure 3. Panel *(a)*: schematics for the problem of particles turning into the perforation. Panels *(b)* and *(c)*: comparison between the model and CFD simulations in Wu and Sharma (2016). Panel *(d)*: comparison between the model and laboratory measurements in Gruesbeck and Collins (1982).

The perforation slurry flow rates into perforations are calculated based on the perforation pressure drop as

$$\sum_{j=1}^{N_p} q_j^s = q_0^s, \Delta p_p = \sigma_j + \frac{\rho_f \left(q_j^s\right)^2}{2 C_j^2 A_j^2}, j = 1..N_p. \tag{3}$$

Here N_p is the number of perforations, Δp_p is the unknown perforation pressure drop, $A_j = \pi\, d_p^2/4$ is perforation area, σ_j is the stress shadow, while C_j is the discharge coefficient for jth perforation. The solution of the above equation (3) gives the perforation slurry flow rates q_p^s, and also yields the distribution of the average wellbore velocity v_w along the well. For the general case when there is non-trivial stress shadow, equations (3) are solved numerically using an iterative procedure.

It is instructive to outline the phasing optimization procedure summarized in Dontsov et al. (2023). First, the slurry distribution between the perforations is determined exclusively by (3); the answer is independent on the perforation phasing. As the slurry flows downstream from perforation to another perforation, the question is how to optimally select the azimuth of the perforation to achieve an overall more uniform proppant distribution between the holes. One possibility is to require that the particle concentration entering the perforation is the same as the average particle concentration in the wellbore. With reference to Fig. 1, the proppant turning always reduces the amount of proppant that enters the perforation. However, due to gravity, there is higher proppant concentration at the bottom of the well. Therefore, if the perforation is located in the lower part of the well, then the loss of concentration due to inability to turn into perforation can be compensated by the increased local particle concentration. Consequently, as shown in Dontsov et al. (2023), the optimal phasing transitions from the bottom of the well for the heel part of the stage to approximately middle of the well for the toe part of the stage. In this case, the proppant distribution between individual perforations can be made more uniform. Under some circumstances, the proppant distribution can be made perfectly uniform. An alternative optimization is also considered, in which all perforations have the same orientation whose value is optimized. As shown in Dontsov et al. (2023), the result for the optimal phasing also falls into the lower part of the wellbore, albeit it is closer to the side than the bottom.

Results

In order to understand the influence of uncertainty on particle distribution between perforations, a field-scale case is considered as an example. The input parameters correspond to the test case PTST2 from Snider et al. (2022) with 100 mesh proppant. The input parameters are summarized in Fig. 4. The original design has 13 clusters with 3 perforations per cluster with 120° difference in phasing. Perforation diameter is given a uniformly distributed uncertainty of 0.03 in, and phasing is given a uniformly distributed uncertainty of 10°. A total of 1000 random realizations are calculated to obtain the statistical distribution of the results. In addition, stress shadow from the previous stage is added. It is calculated based on the assumption that the fracture has constant height of 200 ft and the net pressure is 600 psi, see, e.g., Wu and Olson (2015) for the equation to calculate such a stress shadow.

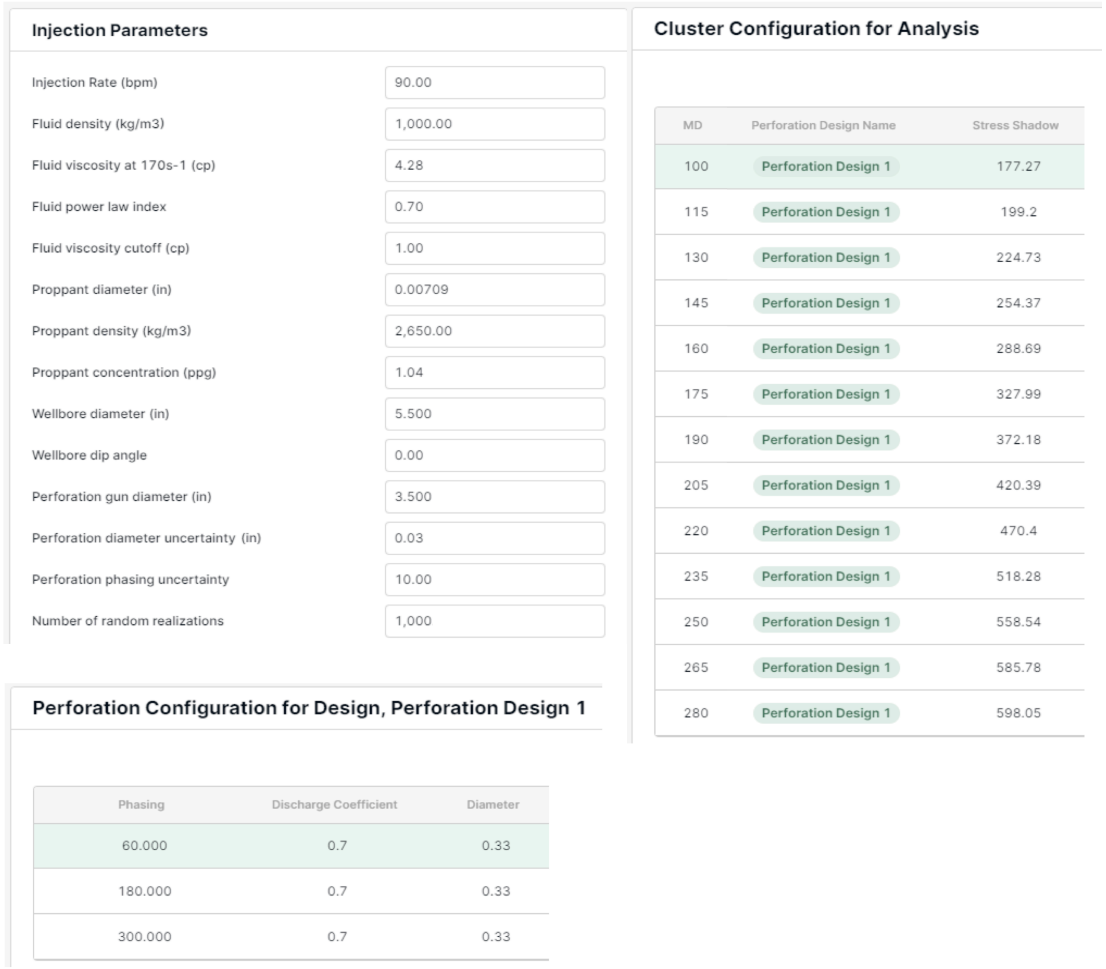

Figure 4. Input parameters for the example calculation.

Figs. 5-10 plot results of numerical simulations for various scenarios. Panels *(a)* on all figures show the variation of proppant rate (slurry rate times the volume fraction), slurry rate, as well as the gun centered perforation phasing versus perforation number. The proppant and slurry rates are also averaged over the cluster and the results are shown by the gray lines. The markers represent the result averaged over all 1000 realizations, while the error bars indicate standard deviation. In addition, Fig. 5 also plots the measurements from Snider et al. (2022) by the red lines with circular markers. Panels *(b)* on all figures show the distribution of the coefficient of variation (standard deviation divided by mean) for proppant and slurry at the perforation and cluster level. All 1000 realizations are shown on histograms. The value of the coefficient of variation for each realization quantifies uniformity of proppant and slurry distribution

between perforations or clusters. If such a coefficient is equal to zero, then the distribution is perfectly uniform. The dashed gray lines indicate the average value of the coefficient of variation and the number shows the actual numeric value.

Fig. 5 shows the results of simulations for the input parameters summarized in Fig. 4, but without stress shadow. It also compares the result to the measurements from Snider et al. (2022). More comparisons with other experimental cases can be found in Dontsov (2023). As can be seen from the results, there is a good level of agreement between the model and the measurements. The variation of the proppant rate is smaller in the heel part of the stage and increases towards the toe part of the stage. The slurry rate is practically uniform, when considering the average over 1000 realizations. However, the variation of perforation diameter introduces noticeable variation of the slurry rate for each individual case. Coefficient of variation of proppant at perforation level is high, with the average of 0.63. This is because perforations with different orientations receive significantly different amount of proppant towards the toe of the stage. Once the average over the perforation cluster is considered, the average coefficient of variation drops to 0.19, but it is still relatively high. The coefficient of variation for slurry is much smaller and averages to 0.10 at the perforation level and to 0.057 at the cluster level. Note that such a variation is caused exclusively by the uncertainty of the perforation diameter. In the ideal case of no uncertainty, all perforations have the same diameter and the resultant slurry distribution is perfectly uniform.

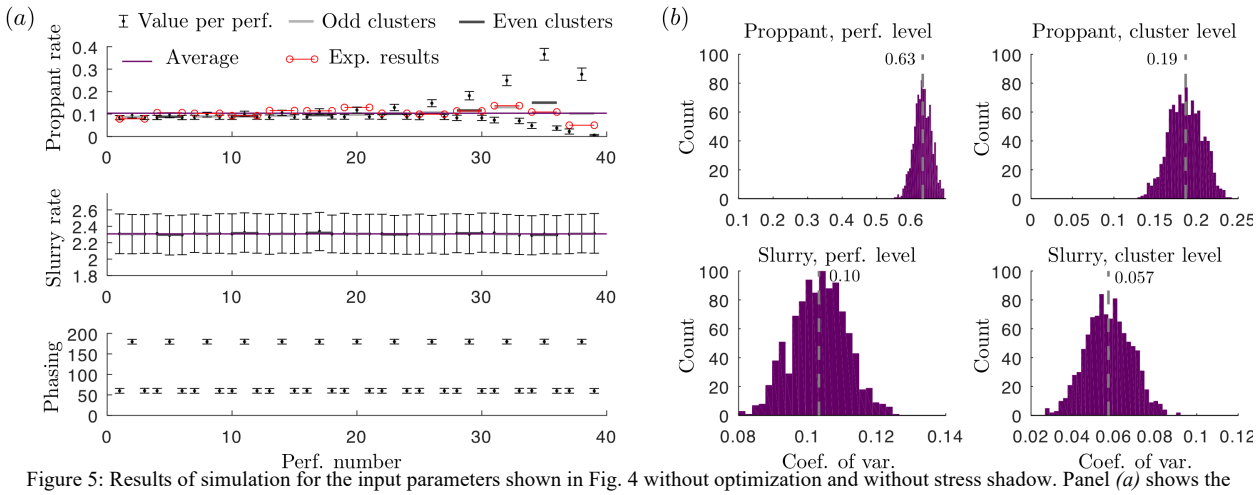

Figure 5: Results of simulation for the input parameters shown in Fig. 4 without optimization and without stress shadow. Panel *(a)* shows the proppant rate, slurry rate, and phasing versus perforation number. Panel *(b)* shows the coefficient of variation for proppant and slurry at the perforation and cluster levels.

Fig. 6 shows the case without stress shadow, but the azimuth of each individual perforation is optimized according to the algorithm presented in Dontsov et al. (2023). The optimal phasing gradually descends from 180°, i.e., the bottom of the well, to approximately 90°, i.e., the side of the well. Note that these numbers for the phasing are gun centered, which is in contrast to the numbers reported in Dontsov et al. (2023), which are well centered. The resultant proppant rate is much more uniform (notice a different scale for the y axis compared to Fig. 5). In addition, the variation of the proppant rate for different perforations is also greatly reduced. The slurry distribution did not visually change. Coefficient of variation of proppant dropped significantly to the average of 0.16 at the perforation level and to 0.094 at the cluster level. This represents an improvement of almost 4 times at the perforation level and 2 times at the cluster level relative to the original non-optimized perforation configuration. The coefficient of variation for slurry is the same as for the previous case since perforation phasing does not affect slurry distribution.

Fig. 7 shows the case without stress shadow, for which all perforations are assumed to have the same orientation, which is optimized. Note that each perforation has its own value of the uncertain phasing, with the mean equal to the optimized value. As can be seen from the figure, this case results in less uniform proppant distribution between clusters, while the slurry distribution is unchanged. The optimal

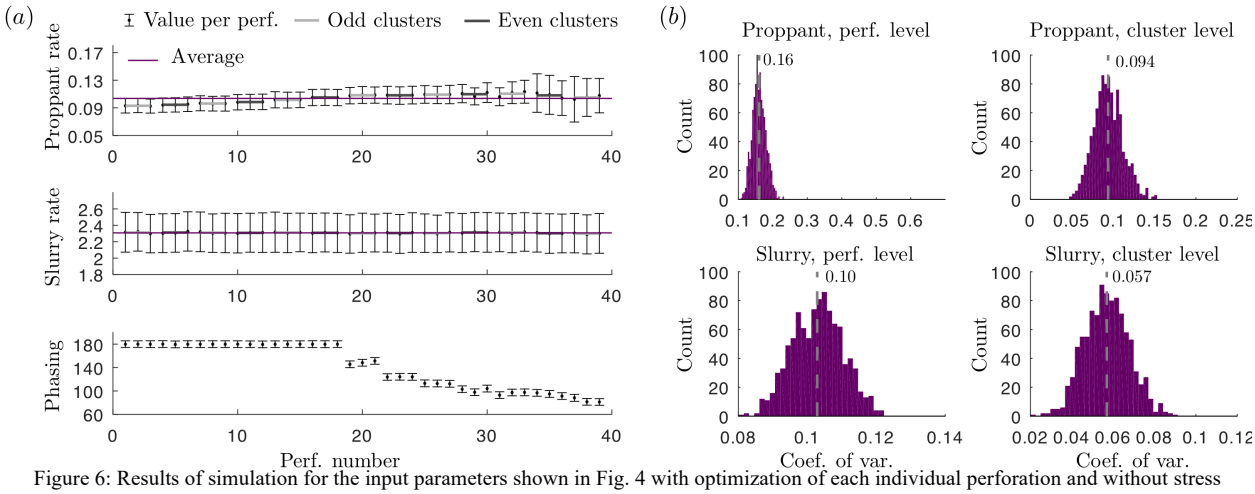

Figure 6: Results of simulation for the input parameters shown in Fig. 4 with optimization of each individual perforation and without stress shadow. Panel *(a)* shows the proppant rate, slurry rate, and phasing versus perforation number. Panel *(b)* shows the coefficient of variation for proppant and slurry at the perforation and cluster levels.

value of perforation azimuth is approximately 93°. As was mentioned before, this number is for gun centered phasing, which is in contrast to the result reported in Dontsov et al. (2023), which assumes well centered phasing. Looking at the distributions, we can conclude that such single degree of freedom optimization is less efficient compared to the previous case, but it still leads to a much more uniform proppant distribution compared to the original case shown in Fig. 5. The coefficient of variation for proppant is 0.20 at the perforation level and 0.14 at the cluster level.

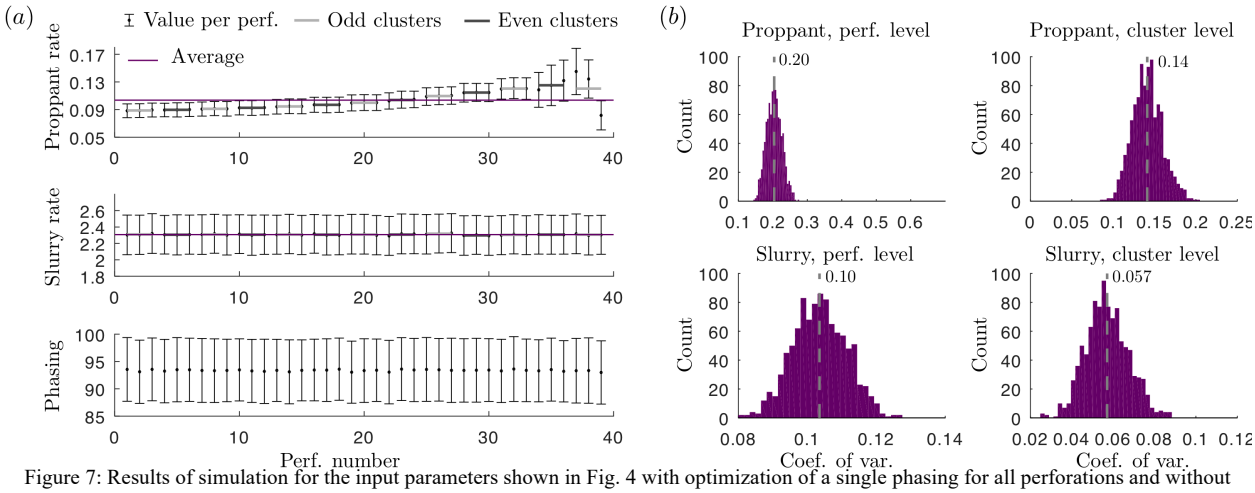

Figure 7: Results of simulation for the input parameters shown in Fig. 4 with optimization of a single phasing for all perforations and without stress shadow. Panel *(a)* shows the proppant rate, slurry rate, and phasing versus perforation number. Panel *(b)* shows the coefficient of variation for proppant and slurry at the perforation and cluster levels.

Fig. 8 shows the original case (see Fig. 5), but now with stress shadow. The addition of stress shadow affects the slurry distribution between the perforations, which is evident from the slurry rate plot. More volume of slurry enters the heel clusters and less slurry enters the toe clusters. The behavior of proppant is qualitatively the same as for the original case in Fig. 5. The average coefficient of variation of proppant actually reduced. This is because higher proppant concentrations typically occur in toe clusters, but since the slurry rate is reduced, this effectively reduces the amount of proppant that enters the toe clusters, which makes the overall proppant distribution more uniform. Coefficient of variation of slurry increased marginally compared to the original case in Fig. 5, even though the qualitative behavior of the average slurry rate within the stage changed noticeably.

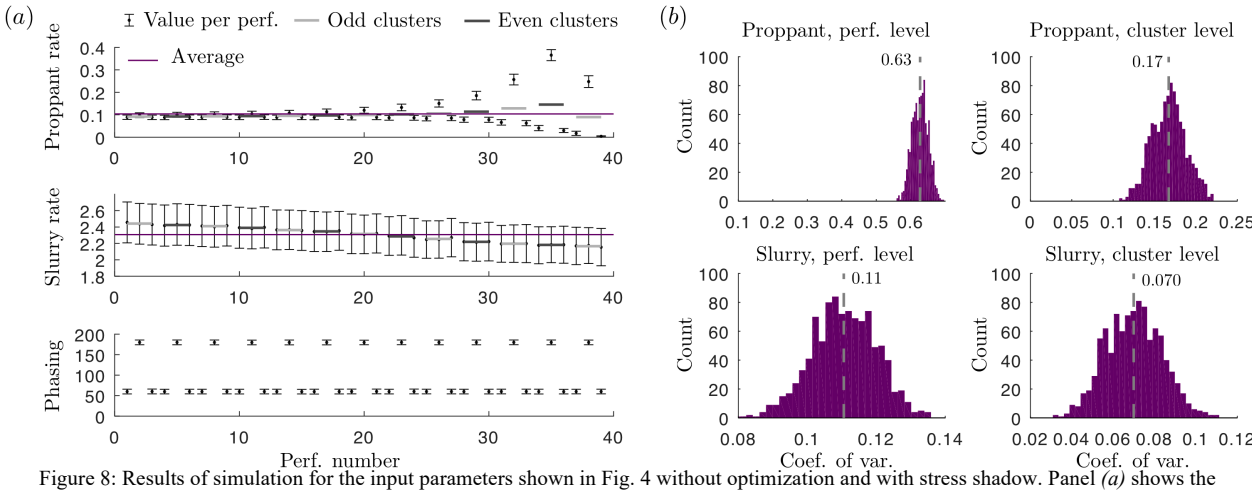

Figure 8: Results of simulation for the input parameters shown in Fig. 4 without optimization and with stress shadow. Panel *(a)* shows the proppant rate, slurry rate, and phasing versus perforation number. Panel *(b)* shows the coefficient of variation for proppant and slurry at the perforation and cluster levels.

Fig. 9 shows the case with the optimization of each individual perforation (see Fig. 6), but now with stress shadow. Optimal phasing remains practically the same and proppant distribution is more uniform compared to the result in Fig. 6. The reason is the same as for the previous case, namely, lower slurry rates at the toe of the stage reduce the amount of proppant there, which was initially above average. The slurry distribution is practically the same as for the previous case.

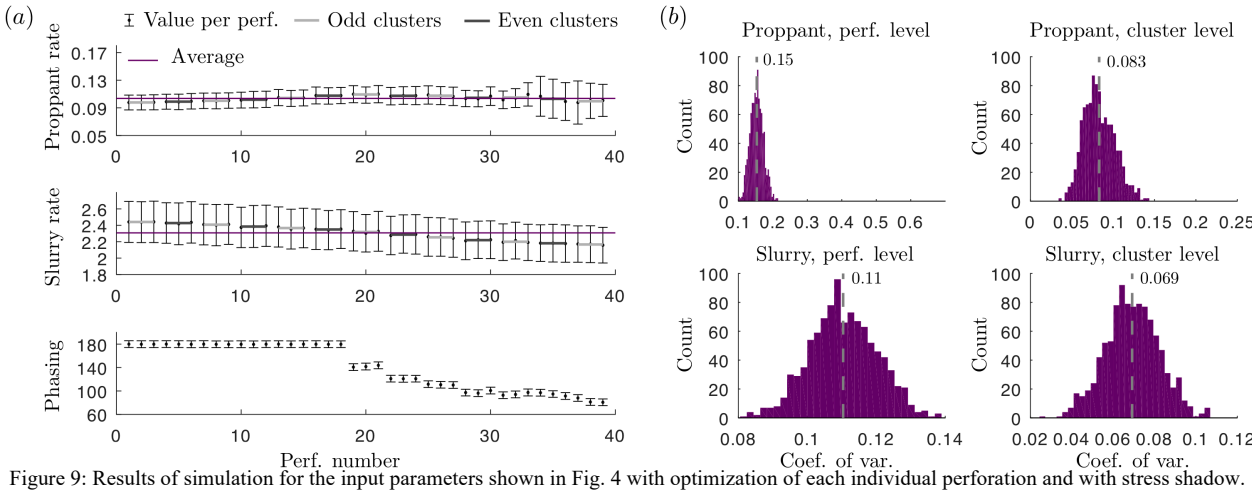

Figure 9: Results of simulation for the input parameters shown in Fig. 4 with optimization of each individual perforation and with stress shadow. Panel *(a)* shows the proppant rate, slurry rate, and phasing versus perforation number. Panel *(b)* shows the coefficient of variation for proppant and slurry at the perforation and cluster levels.

Fig. 10 shows the case for which all perforations are assumed to have the same orientation, but now with stress shadow. Compared to the original case without stress shadow shown in Fig. 7, the slurry rate becomes less uniform, but the proppant distribution is more uniform. The optimal phasing is also practically the same. In addition, the difference with the case, for which azimuth of each perforation is optimized, becomes marginal. Thus, the addition of uncertainty and stress shadow makes the performance of the single oriented perforation design comparable to the more complex case, for which each cluster has unique perforation orientation.

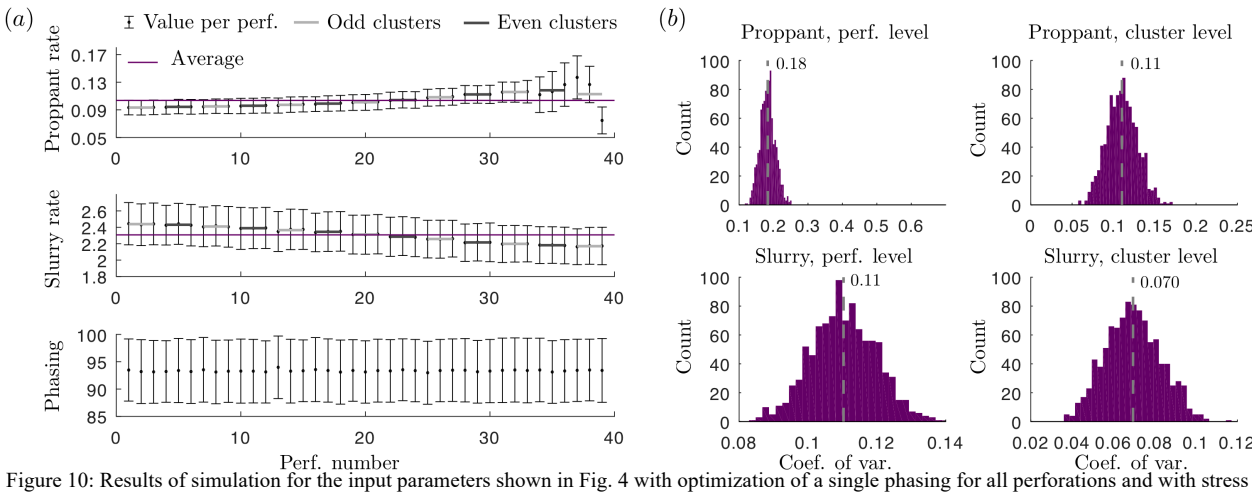

Figure 10: Results of simulation for the input parameters shown in Fig. 4 with optimization of a single phasing for all perforations and with stress shadow. Panel *(a)* shows the proppant rate, slurry rate, and phasing versus perforation number. Panel *(b)* shows the coefficient of variation for proppant and slurry at the perforation and cluster levels.

Conclusions

This paper investigates the problem of proppant distribution between perforations in view of uncertainties of perforation phasing and diameter. First, a brief overview of the proppant-wellbore dynamics model used for the analysis is presented. The model assumes that particle distribution in the well can be non-uniform due to gravity and also accounts for the particle inertia effect, which leads to some particles to miss the perforation. Comparison with laboratory and computational data is presented to validate the model. Perforation erosion is not considered in the model at this stage.

A field scale case consisting of 13 clusters is considered. The original perforation design has 3 holes with 120° phasing. Two types of phasing optimization are considered. In the first one, phasing of each individual perforation is optimized towards achieving more uniform proppant distribution between perforations. In the second optimization approach, a single value of perforation azimuth for all clusters is selected and it is then optimized. An uncertainty is added to perforation phasing and diameter and the results are presented in terms of the statistical distribution of proppant and slurry uniformity. In addition, the results with and without stress shadow from previous stage are compared.

The findings demonstrate that the original perforation design with 120° phasing leads to a significant variation of the amount of proppant received by each individual perforation. Optimization of perforation azimuth for each individual perforation leads to the best result and significantly improves uniformity of proppant distribution. The optimal phasing ranges from 180° at the heel to approximately 90° at the toe of the stage. When oriented perforation is employed and all clusters are required to have the same optimal azimuth, then the uniformity of proppant is still greatly improved relative to the original case, albeit it is slightly worse compared to the case in which phasing of each perforation is optimized. The optimal phasing in this case is slightly above 90°. The addition of stress shadow leads to the non-uniform slurry distribution, so that the heel clusters receive more slurry and the toe clusters receive less slurry. This in part balances the non-uniform proppant distribution for all cases, since the toe clusters tend to receive more proppant on average. Thus, counterintuitively, stress shadow from the previous stage makes it somewhat easier to achieve a uniform proppant distribution between clusters, even though it causes the slurry distribution to be less uniform.

Acknowledgements

The authors would like to acknowledge Dr. Cramer from ConocoPhillips for emphasizing the importance of parameter uncertainty for perforation cluster design.

References

Ahmad, F. 2020. *Experimental investigation of proppant transport and behavior in horizontal wellbores using low viscosity fluids*. PhD thesis, Colorado School of Mines, Golden, Colorado.

Ahmad, F., and Miskimins, J. 2019a. Proppant transport and behavior in horizontal wellbores using low viscosity fluids. In Proceedings of Hydraulic Fracturing Technology Resources Conference, Houston, Texas, 5-7 February. SPE-194379-MS.

Ahmad, F., and Miskimins, J. 2019b. An experimental investigation of proppant transport in high loading friction-reduced systems utilizing a horizontal wellbore apparatus. In Proceedings of Unconventional Resources Technology Conference, Denver, Colorado, USA, 22-24 July. URTEC-2019-414-MS.

Ahmad, F., Miskimins, J., Liu, X., Singh, A., and Wang, J. 2021. Experimental investigation of proppant placement in multiple perforation clusters for horizontal fracturing applications. In Proceedings of Unconventional Resources Technology Conference, Houston, Texas, USA, 26-28 July. URTEC-2021-5298-MS.

Cramer, D. D. 1987, The application of limited-entry techniques in massive hydraulic fracturing treatments. In Proceedings of the SPE Production Operations Symposium, Oklahoma City, Oklahoma, USA, 8-10 March. SPE-16189.

Crespo, F., Aven, N., Cortez, J., Soliman, M. Y., Bokane, A., Jain, S., and Deshpande, Y. 2013. Proppant distribution in multistage hydraulic fractured wells: A large-scale inside-casing investigation. In Proceedings of Hydraulic Fracturing Technology Resources Conference, 4-6 February 2013, Houston, Texas, USA. SPE-163856-MS.

Dontsov, E. 2023. A model for proppant dynamics in a perforated wellbore. *arXiv:2301.10855*.

Dontsov, E., Hewson, C., and McClure, M. 2023. A model for optimizing proppant distribution between perforations. In American Rock Mechanics Association, Atlanta, GA. ARMA 23-348.

Gillies, R. 1993. *Pipeline flow of coarse particle slurries*. PhD thesis, University of Saskatchewan, Saskatoon, Saskatchewan.

Gruesbeck, C. and Collins, R. E. 1982. Particle transport through perforations. *Society of Petroleum Engineers Journal*, 22 (06):857–865.

Kolle, J., Mueller, A., Baumgartner, S., and Cuthill, D. 2022. Modeling proppant transport in casing and perforations based on proppant transport surface tests. In Proceedings of Hydraulic Fracturing Technology Resources Conference, 1-3 February 2022, Houston, Texas, USA. SPE-209178-MS.

Ngameni, K. 2016. Proppant transport in horizontal wellbores using fresh water. Master's thesis, Colorado School of Mines, Golden, Colorado.

Ngameni, K. L., Miskimins, J. L., Abass, H. H., and Cherrian, B. 2017. Experimental study of proppant transport in horizontal wellbore using fresh water. In Proceedings of Hydraulic Fracturing Technology Resources Conference, 24-26 January 2017, Houston, Texas, USA. SPE-184841-MS.

Snider, P., Baumgartner, S., Mayerhofer, M., and Woltz, M. 2022. Execution and learnings from the first two surface tests replicating unconventional fracturing and proppant transport. In Proceedings of Hydraulic Fracturing Technology Resources Conference, 1-3 February 2022, Houston, Texas, USA. SPE-209141-MS.

Wu, C. 2018. *Modeling Particulate Flows in Conduits and Porous Media*. PhD thesis, University of Texas at Austin, Austin, Texas.

Wu, C.-H., and Sharma, M. 2016. Effect of perforation geometry and orientation on proppant placement in perforation clusters in a horizontal well. In Proceedings of Hydraulic Fracturing Technology Resources Conference, 9-11 February 2016, Houston, Texas, USA. SPE-179117-MS.

Wu, K., and Olson, J. 2015. A simplified three-dimensional displacement discontinuity method for multiple fracture simulations. *Int. J. Fract.*, 193:191–204.